Original Article

Effects of different severities of disc degeneration on the range of motion of cervical spine

ABSTRACT

Aims and Objectives: The human spine degenerates with age. Intervertebral disc degeneration occurs in the cervical spine. The objective of this study is to determine the effects of degenerative disc diseases on the range of motion (ROM) of the human cervical spinal column using a validated finite-element model.

Materials and Methods: The validated intact and healthy C2–T1 finite-element model simulated the cortical shell, cancellous core, posterior elements of the vertebrae, and spinal ligaments (longitudinal, capsular, spinous and ligamentum flava, and nucleus and annulus of the discs). Three different stages of the disc disease, that is, mild, moderate, and severe, were simulated at the C5–C6, C6–C7, and C5–C6–C7 discs, respectively, and they were termed as upper single level, lower single level, and bi-level (BL) models, respectively. The material properties and geometry of the disc(s) were altered to simulate the different stages of degeneration. The external mechanical loading was applied in the sagittal mode, via flexion–extension motions and the magnitude was 2.0 Nm for each mode. They were applied to each of the healthy and disc degeneration models, and for each of the three severities of degeneration. The ROM at adjacent and index levels was extracted and normalized with respect to the healthy (baseline) spine.

Results: A nonuniform distribution in the ROM was found for different disc degeneration states, segmental levels, and flexion–extension loading modes. The specific results for each and level are reported in the results section of the paper.

Conclusion: Closer follow-up times may be necessary in symptomatic patients with progressive disease, especially with BL involvements.

Keywords: Adjacent segment, cervical spine, degenerative disc disease, finite-element model, range of motion

INTRODUCTION

The human spine shows signs of degeneration/disease over time. Degenerative disc disease (DDD) is attributed to the supporting head mass and motions that occur in the adult cervical spinal column. While human cadaver experimental models have been used to evaluate their role on the biomechanics, numerical modeling tools are gaining more importance, especially finite-element models, because of their parametrization abilities and ability to simulate different severities of disc degeneration on the same model.[1] The objective of the present study is to determine the effects of DDD on the index and adjacent segment range of motions (ROMs) of the human cervical spine using a validated finite-element model.

Narayan Yoganandan[1], Hoon Choi[1], Yuvaraj Purushothaman[1,2], Davidson Jebaseelan[2], Jamie Baisden[1], Shekar Kurpad[1]

[1]Center for NeuroTrauma Research, Department of Neurosurgery, Medical College of Wisconsin, Milwaukee, WI, USA, [2]Department/School of Mechanical Engineering, Vellore Institute of Technology, Chennai Campus, Chennai, Tamil Nadu, India

Address for correspondence: Prof. Narayan Yoganandan, Department of Neurosurgery, Medical College of Wisconsin, Milwaukee, 8701 Watertown Plank Road, WI 53226, USA. E-mail: yoga@mcw.edu

Access this article online	
Website: www.jcvjs.com	**Quick Response Code**
DOI: 10.4103/jcvjs.JCVJS_158_20	

How to cite this article: Yoganandan N, Choi H, Purushothaman Y, Jebaseelan D, Baisden J, Kurpad S. Effects of different severities of disc degeneration on the range of motion of cervical spine. J Craniovert Jun Spine 2020;11:269-75.

MATERIALS AND METHODS

Finite-element model

The human cervical spine (C2–T1) finite-element model included the hard- and soft-tissue components of the osteo-ligamentous column and the surrounding musculature. The column simulated the subaxial vertebrae including the dens of the axis and posterior complexes: pedicles, laminae, and spinous processes. The anterior longitudinal ligament, posterior longitudinal ligament, capsular ligaments of the facet articulations, ligamentum flavum, and inter- and supraspinous ligaments connected the vertebrae at their respective anatomical locations. The intervertebral discs simulated their annulus and nucleus components: the latter component was asymmetrically placed inside the disc volume, paralleling human anatomy.[2,3] The cortical shell and trabecular core of the vertebral bodies were simulated using shell and hexahedral solid elements, and both had isotropic material properties.[4-7] The endplates and cartilage were simulated by shell elements with linear elastic properties.[8] The annulus ground substance and its fibers, oriented at 45–60°, were simulated by hexahedral solid and membrane elements, with foam and orthotropic properties, and the nucleus was simulated by hexahedral solid elements with viscoelastic material properties.[8-12] The spinal ligaments were simulated using quadrilateral membrane elements with no resistance in compression and nonlinear rate-dependent stress–strain relationships derived from force–displacement relationships of the human cervical spine ligaments.[13,14] Figure 1 shows the finite-element model of the cervical spine used in the study. Table 1 provides the details of the model.

Disease states

The intact spinal column model was modified to accommodate different DDD states, namely mild, moderate, and severe. They were simulated at the C5–C6, C6–C7, and C5–C6–C7 vertebral levels, termed as upper single level (USL), lower single level (LSL), and bi-level (BL) models, respectively. To simulate the mild level of disc disease, the elastic modulus of the nucleus pulposus was assumed to be twice the elastic modulus of the annulus ground substance used in the healthy cervical spinal column, while the properties of the other components remained the same as in the healthy spine model.[15] To simulate the moderate disc disease, in addition to the above change, the elastic modulus of the annulus ground substance was assigned two times the value of the modulus of the annulus ground substance used in the healthy spine model. In addition, the annulus fiber volume was reduced by 25% from the value used in the healthy spine model.[15] To simulate the severely diseased disc, in addition to these changes, the intervertebral disc height was reduced to 85%, of the data used in the healthy cervical spinal model. This approach was also used in the previously cited study. Further rationale for the selection is given in the discussion section.

Loading

The healthy cervical spinal column model was subjected to loads in the sagittal plane: flexion and extension moments of 2 Nm each. They were applied at the cephalad end, and the caudal-most level was fixed in all degrees of freedom. The resulting overall and segmental ROMs were obtained. The flexion and extension moments that produced the overall rotation angles to those of the healthy cervical spinal column were applied to all the diseased spine models. The ROMs were extracted at all subaxial levels for each case, namely, three disease states (mild, moderate, and severe) and three levels (USL, LSL, and BL). The ROM data for the multiple
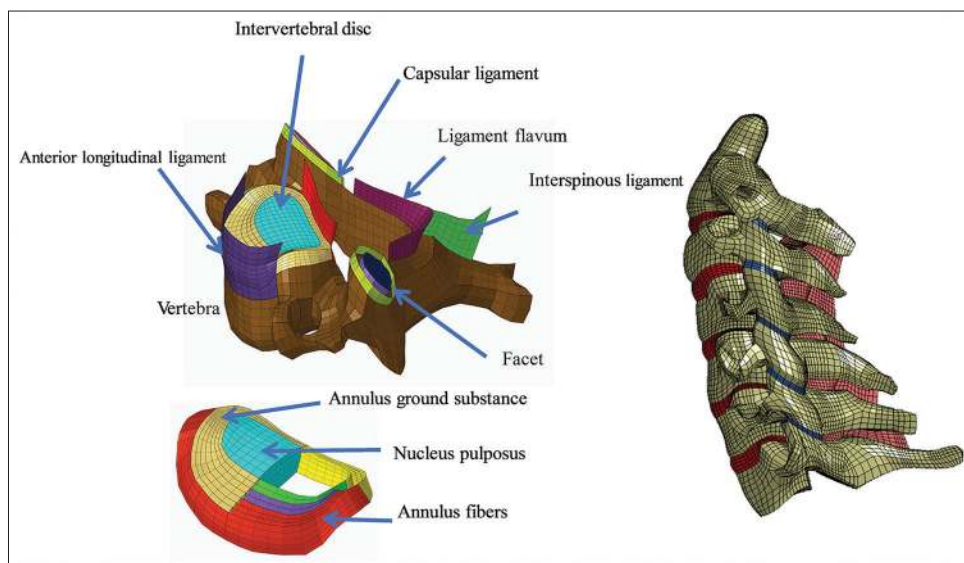

Figure 1: Finite-element model with the details of components. See text for details

models were normalized with respect to the healthy model, that is, no intervertebral disc disease. The results of the normalized changes in the ROMs at the superior and inferior adjacent spinal levels for all cases are as follows: for the USL model, they were at the C4–C5 and C6–C7 levels; for the LSL model, they were at the C5–C6 and C7–T1 levels; and for the BL model, they were at the C4–C5 and C7–T1 levels. The normalization was done using the following equation:

$$NROM = \frac{ROM_d - ROM_h}{ROM_h}$$

where the subscripts *d* and *h* refer to the disease and healthy spine states, respectively, *N* refers to the normalized value, and *ROM* refers to the ROM at the superior or inferior adjacent levels. To minimize repetition, caudal and inferior and cephalad and superior are used interchangeably in this manuscript.

RESULTS

Normalized range of motion from diseased discs at the superior level

Figure 2 shows the normalized ROM in flexion at the superior spinal level for the three diseased states and levels. For the mildly diseased disc(s) for the USL, LSL, and BL spines, the ROM increased from 3.2% to 3.5%; for the moderately diseased disc(s), it increased from 7.8% to 13.9%; and for the severely diseased disc(s), it increased from 9.9% to 33.0%.

Figure 3 shows the normalized ROM in extension at the superior spinal level for the three diseased states and levels. For the mildly diseased disc(s) for the USL, LSL, and BL spines, the ROM increased from 0.4% to 5.8%; for the moderately diseased disc(s), it increased from 3.6% to 6.7%; and for the severely diseased disc(s), it increased from 12.9% to 17.3%.

Normalized range of motion from diseased discs at the inferior level

Figure 2 shows the normalized ROM in flexion at the inferior spinal level for the three diseased states and levels. For the mildly diseased disc(s) for the USL, LSL, and BL spines, the ROM increased from 4.2% to 7.8%; for the moderately diseased disc(s), it increased from 10.0% to 16.8%; and for the severely diseased disc(s), it increased from 25.8% to 36.4%.

Figure 3 shows the normalized ROM at the inferior spinal level in extension for the three diseased states and levels. For the mildly diseased disc(s) for the USL, LSL, and BL spines, the ROM increased from 2.8% to 9.6%; for the moderately diseased disc(s), it increased from 5.3% to 12.9%; and for the severely diseased disc(s), it increased from 15.7% to 21.8%.

Normalized range of motion from diseased discs at the index level

The index level(s) corresponds to the diseased disc level(s): one segment for the USL and LSL and two segments for the BL spines. Figure 2 shows the normalized ROM in flexion for the three diseased states and levels. For the mildly diseased disc(s) for the USL, LSL, and BL spines, the ROM decreased from 7.4% to 10.4%; for the moderately diseased disc(s), it decreased from 22.6% to 27.1%; and for the severely diseased disc (s), it decreased from 51.1% to 56.8%. The decrease in motion for the BL spines was averaged for the two levels. For the BL spine, the decrease was 1.1–2.2 times at the cephalad index level.

Figure 3 shows the normalized ROM in extension for the three diseased states and levels. For the mildly diseased disc(s) for the USL, LSL, and BL spines, the ROM decreased from 3.7% to 8.4%; for the moderately diseased disc(s), it decreased from 14.4% to 16.2%; and for the severely diseased disc(s),
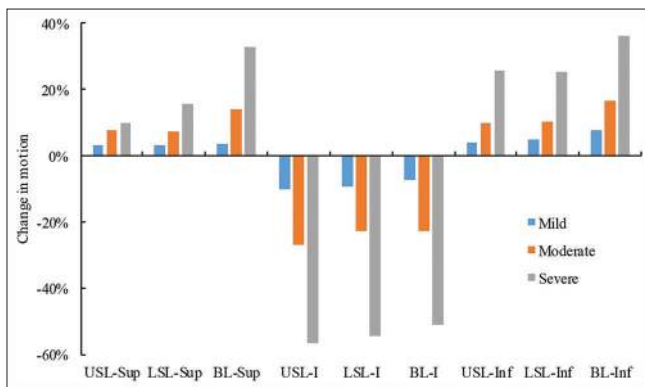

Figure 2: Normalized change in range of motion at the superior (left three sets of three bars), index (middle three sets of three bars), and inferior (three left sets of three bars) levels under flexion and for different disc degeneration severities
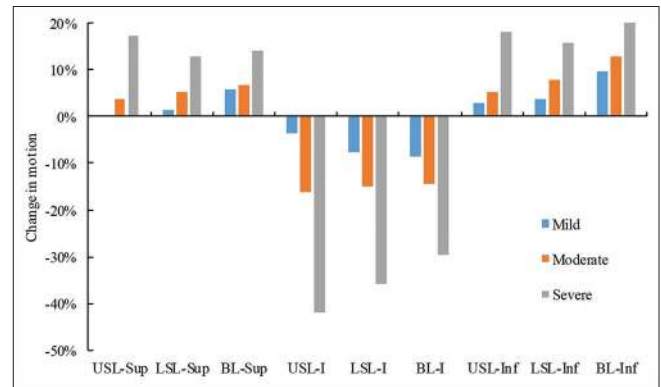

Figure 3: Normalized change in range of motion at the superior (left three sets of three bars), index (middle three sets of three bars), and inferior (three left sets of three bars) levels under extension and for different disc degeneration severities

Table 1: Details of the finite element model used in the study

Component	Element type	Constitutive model	Parameters
Cortical bone	Quadrilateral shell	Isotropic linear elastic	$E=16.8$ GPa, $\mu=0.3$
Trabecular bone	Hexahedral solid	Isotropic linear elastic	$E=0.4$ GPa, $\mu=0.3$
Endplate	Quadrilateral shell	Isotropic linear elastic	$E=5.6$ GPa, $\mu=0.3$
Facet cartilage	Quadrilateral shell	Isotropic linear elastic	$E=0.01$ GPa, $\mu=0.3$
Annulus ground substance	Hexahedral solid	Hill foam	$n=2$, $C1=0.000115$ GPa $C2=0.002101$ GPa $C3=-0.000893$ MPa $b1=4$, $b2=-1$, $b1=-2$
Annulus fibrosus	Quadrilateral membrane	Orthotropic nonlinear elastic	Fiber angle (45°–60°)
Nucleus	Hexahedral solid	Fluid	$K=1720$ MPa
Ligaments	Quadrilateral membrane	Nonlinear properties	Stress-strain curves

μ - Poisson's ratio

it decreased from 29.7% to 41.2%. The decrease in motion for the BL spines was averaged for the two levels. For the BL spine, the decrease was 1.02–1.3 times at the cephalad index level.

DISCUSSION

Disease states
The objective of this study was to determine the effects of different stages or states of DDD on the ROMs of the cervical spine. Disc disease is a multifactorial entity that develops after the full maturation of the cervical spine and is more common with advancing age. Intervertebral discs undergo progressive structural changes in the form of desiccation of the nucleus pulposus and disintegration of the annulus fibrosus, resulting in decreased disc height and osteophyte formation.[1] Radiographic examinations of patients with degenerated spines have shown osteophytes in the presence of reduced disc height.[16,17] These different states of the disc disease affect the biomechanical responses such as the ROM and may lead to spondylosis and neck pain.[18] The mild stage of the disease was simulated by the alteration of the material properties to represent *in vivo* dehydration process of the nucleus pulposus.[19] The moderate stage was simulated by the alteration of the fiber content and material properties of the annulus fibrosus, representing the disintegrated nature of the annulus.[15] The severe stage of the disc disease was simulated by decreasing the disc depth, representing the more advanced stage of degeneration.[20] This initial approach of selecting the three grades of disease process represented the progressive stages of the disease in the human cervical spinal column and were based on the literature.

Choice of spinal levels
The spinal levels considered for the simulations of the disease were at the C5–C6, C6–C7, and C5–C7 levels. The most common level for the appearance of the disease and surgical intervention is at the C5–C6 level.[21] This is followed by its caudal segment. The inclusion of both levels represented more severe and/or two levels of disease that are also common clinically.[3,21,22] These considerations, parallel the prevalence of the disease in the human spine. The ROM was chosen as the metric to describe the biomechanics of the spine which also parallels the clinical assessment as physicians often use this parameter to gauge spinal stability, progression of the disease, and effects on spine functionality from routine radiographs.

Rationale for the choice of material properties
DDD is classified into mild, moderate, and severe categories.[22] The process is sequential/progressive. Mild DDD is characterized by loss of elasticity, termed as nuclear degeneration; moderate DDD is characterized by annulus degradation in addition to nucleus desiccation, termed as annual weakening; and severe DDD is characterized by reduction in the disc height and sometimes accompanied by osteophytes.[23-25] As these are progressive, mild DDD was simulated by doubling the elastic modulus used in the normal spine, accounting for the loss of elasticity. Because the nucleus is the only component to deviate in the mild degeneration category, all the other components' material properties were maintained in the same state as the normal model. For moderate DDD, while specific magnitudes are yet to reach consensus in the spine community, as a first step, the ground substance modulus was doubled, and the fiber volume was decreased by one-quarter from the normal spine, along with the new elastic modulus for the nucleus. These represented annulus degradation. For severe DDD, the disc height was reduced to 85% of its normal height along with the above changes in the annulus and nucleus properties. The values chosen for the material properties for DDD were based on clinical studies and used in another finite modeling study.[15] To introduce the exact material properties of DDD states in the modeling process, additional studies should be conducted. Biomechanical tests can be conducted using human cadaver discs. A plausible design of experiment would be to analyze the biomechanical output as a function of factors such as age, sex,

and disc grade, and examine their interrelationships with the material properties. From the relationship(s), a better estimate of the magnitudes of the material properties can be used in patient-specific finite-element models to assist in clinical decisions. For geometrical changes, however, for example, the disc height for the severe category can be obtained from patient-specific spinal images: X-rays, computed tomography, or magnetic resonance imaging, and directly included in patient-specific models. These are considered as future studies.

Loading

Sagittal plane loading was applied in this study, although loading on the human spine is complex and three dimensional. The center of gravity of the human head lies anterior to the longitudinal axis of the cervical spine, and the sagittal plane of loading is the primary mode in the human head-and-neck system. Recent clinical studies use the sagittal alignment as a measure of patient outcomes.[26] Lateral bending/axial rotation is also a mechanical loading mode on the spine. Axial rotation is primarily borne by the upper head-and-neck junction and little motion is transmitted to the C2–T1 column. This is due to the unique anatomical features: OC–C2 is devoid of discs, while ligaments and facet joints connect to the subaxial spine, and the OC–C1 is a cup-like joint, and C1–C2 is also unique. In addition, in the C2–T1 column, axial rotation is coupled with lateral bending due to the characteristic joint anatomy.[27,28] While the sagittal plane of loading was used to demonstrate the effectiveness of the model, other modes should be applied to fully analyze patient-specific models. They can be done by introducing different loading scenarios in the other planes.

Adjacent segments

Immediate adjacent levels contiguous to the diseased disc level(s) were chosen to evaluate the effects of different stages of disc disease on the spinal response. The superior and inferior levels were different in the three models: the caudal levels were the same in the LSL and BL models, whereas the cephalad levels were the same in the USL and BL models. In addition, the index levels varied, and the results for the BL model were presented as an average of both diseased levels to compare with the USL and LSL models. Only these levels were considered in this study because any effects due to the disc disease first transfer to the immediate superior and inferior segments, and this is in line with clinical concerns, especially during surgical procedures. In fact, adjacent segment disease issues including reoperations are commonly reported in literature.[29-32]

Kinematics

The increase in the spinal mobility (ROM) was <10% at both adjacent levels and in both flexion and extension modes. This was true for all the three conditions: USL, LSL, and BL. At

the index level(s) also, the change was <10% in both modes; however, the motion consistently decreased due to the disease in all conditions. The increase in the spinal mobility was consistently greater than those from the mild degree of disc disease, and this was true for the three conditions and both modes of loading. At the superior adjacent level, the greatest magnitude of 14% and at the inferior level, the greatest value of 17% were associated with the BL condition in flexion. At the index level(s), however, decreases of up 27% in flexion and 16% in extension were apparent from the stress-analysis outputs. The increases in the spinal mobility, as expected, were consistently greater than those from the mild and moderate states of the disease, and these were true for all the three conditions and both modes of loading. Increases were as high as one-third in both adjacent levels in flexion, while they were comparatively lower (up to one-fifth) in extension, for the BL condition. The increase in the magnitudes was lower for the USL and LSL conditions in both modes. This is expected as the disease was confined to a single level in contrast to the BL spine. The decrease in motion at the index levels reached peak magnitudes, approximately one-half in flexion and two-fifth in extension. As severe degeneration may induce or accentuate associated morphological changes (spondylosis, radicular or myelopathic symptoms), these results emphasize the need for more and/or early clinical attention that may include nonconservative options in symptomatic patients. It should be noted that the clinical progression of the symptomatology is not linear and may accelerate as the disease state reaches a critical state, culminating in surgical intervention.

Range of motion

ROM evaluations are routinely done using normal and flexion–extension X-rays taken in a clinical setting. The magnitude of the ROM depends on the patient's symptoms and factors such as the degree of spine degeneration, and any surgical procedures. The exact bending moments acting on the *in vivo* spine are not known; however, *in vivo*-measured motions can be combined with muscular forces to obtain loading estimates. While the present study was not focused on these aspects, inverse dynamics methods can be used to relate motion with *in vivo* loading.[33-39]

It should be noted that flexion–extension loading of 2 Nm has been used in human cadaver and modeling studies as a measure of physiological loading in the *in vivo* human. The validation of the present intact normal degeneration-free spinal model with segmental and overall ROM data from flexion–extension loading of human cadaver spines is an indirect validation of *in vivo* ROM.[40] Human studies are necessary to construct subject-specific spinal models from

images, obtain *in vivo* ROMs based on the current morphology and symptomatology, estimate the loading using inverse dynamics, and exercise the finite-element model for the evaluation of intrinsic and extrinsic biomechanical metrics. This process serves as a clinical tool for personalized medicine. The current article lays a foundation for such pursuits.

Clinical perspectives

While the above discussion stems directly from the reported results, the unique features of the cervical spine will be of value to investigate other issues. For example, patient-specific models are entering the spine field of personalized medicine. Development of biomechanical models of the spine that depict the specific anatomy of the patient is a necessary and an important first step to understand the response of the spine under the current state of the disorder, for example, spondylosis and disc disease states in patients with neck pain.[23,41,42] The present model was developed using multiblock technique.[43,44] The differentiation of the vertebrae into different blocks allows the user to independently control the regional anatomy of the spine, thus achieving the patient-specific spine model using the baseline finite-element model. It should be noted that the baseline model was used for the current analysis of ROMs and osteophytes were not included. The development of the bony growth was deemed to be an advanced stage of the severe disease, and the present model can be extended to simulate this disc status. It can be done by changing the material properties of the local elements of the disc to match the bone growth.

Acknowledgments

Financial support and sponsorship
Nil.

Conflicts of interest
There are no conflicts of interest.

REFERENCES

1. Clark CR. The Cervical Spine. 3rd ed. Philadelphia, PA: Lippincott-Raven; 1998.
2. Mercer S, Bogduk N. The ligaments and annulus fibrosus of human adult cervical intervertebral discs. Spine 1999;24:619-26; discussion 27-8.
3. Tonetti J, Potton L, Riboud R, Peoc'h M, Passagia JG, Chirossel JP. Morphological cervical disc analysis applied to traumatic and degenerative lesions. Surg Radiol Anat 2005;27:192-200.
4. Reilly DT, Burstein AH. The elastic and ultimate properties of compact bone tissue. J Biomech 1975;8:393-405.
5. Reilly DT, Burstein AH, Frankel VH. The elastic modulus for bone. J Biomech 1974;7:271-5.
6. Kopperdahl DL, Keaveny TM. Yield strain behavior of trabecular bone. J Biomech 1998;31:601-8.
7. Östh J, Brolin K, Svensson MY, Linder A. A female ligamentous cervical spine finite element model validated for physiological loads. J Biomech Eng 2016;138:061005.
8. Panzer MB, Cronin DS. C4-C5 segment finite element model development, validation, and load-sharing investigation. J Biomech 2009;42:480-90.
9. Cassidy JJ, Hiltner A, Baer E. Hierarchical structure of the intervertebral disc. Connect Tissue Res 1989;23:75-88.
10. Holzapfel GA, Schulze-Bauer CA, Feigl G, Regitnig P. Single lamellar mechanics of the human lumbar annulus fibrosus. Biomech Model Mechanobiol 2005;3:125-40.
11. Iatridis JC, Setton LA, Foster RJ, Rawlins BA, Weidenbaum M, Mow VC. Degeneration affects the anisotropic and nonlinear behaviors of human annulus fibrosus in compression. J Biomech 1998;31:535-44.
12. Iatridis JC, Weidenbaum M, Setton LA, Mow VC. Is the nucleus pulposus a solid or a fluid? Mechanical behaviors of the nucleus pulposus of the human intervertebral disc. Spine (Phila Pa 1976) 1996;21:1174-84.
13. Mattucci SF, Moulton JA, Chandrashekar N, Cronin DS. Strain rate dependent properties of human craniovertebral ligaments. J Mech Behav Biomed Mater 2013;23:71-9.
14. Yoganandan N, Kumaresan S, Pintar FA. Geometric and mechanical properties of human cervical spine ligaments. J Biomech Eng 2000;122:623-9.
15. Kumaresan S, Yoganandan N, Pintar FA, Maiman DJ, Goel VK. Contribution of disc degeneration to osteophyte formation in the cervical spine: A biomechanical investigation. J Orthop Res 2001;19:977-84.
16. Buckwalter JA. Aging and degeneration of the human intervertebral disc. Spine (Phila Pa 1976) 1995;20:1307-14.
17. Ghosh P. Biology of the Intervertebral Disc. Boca Raton, FL: CRC Press; 1988.
18. Ang BO, Monnier A, Harms-Ringdahl K. Neck/shoulder exercise for neck pain in air force helicopter pilots: A randomized controlled trial. Spine (Phila Pa 1976) 2009;34:E544-51.
19. Kim YE, Goel VK, Weinstein JN, Lim TH. Effect of disc degeneration at one level on the adjacent level in axial mode. Spine (Phila Pa 1976) 1991;16:331-5.
20. Friedenberg ZB, Miller WT. Degenerative disc disease of the cervical spine. J Bone Joint Surg Am 1963;45:1171-8.
21. Teraguchi M, Yoshimura N, Hashizume H, Muraki S, Yamada H, Minamide A, *et al*. Prevalence and distribution of intervertebral disc degeneration over the entire spine in a population-based cohort: The Wakayama Spine Study. Osteoarthritis Cartilage 2014;22:104-10.
22. Suzuki A, Daubs MD, Hayashi T, Ruangchainikom M, Xiong C, Phan K, *et al*. Patterns of cervical disc degeneration: Analysis of magnetic resonance imaging of over 1000 symptomatic subjects. Global Spine J 2018;8:254-9.
23. Lestini WF, Wiesel SW. The pathogenesis of cervical spondylosis. Clin Orthop Relat Res 1989 Feb 239:69-93.
24. Nathan H. Compression of the sympathetic trunk by osteophytes of the vertebral column in the abdomen: An anatomical study with pathological and clinical considerations. Surgery 1968;63:609-25.
25. Shedid D, Benzel EC. Cervical spondylosis anatomy: Pathophysiology and biomechanics. Neurosurgery 2007;60:S7-13.
26. Hyun SJ, Kim KJ, Jahng TA, Kim HJ. Relationship between T1 slope and cervical alignment following multilevel posterior cervical fusion

surgery: Impact of T1 slope minus cervical lordosis. Spine (Phila Pa 1976) 2016;41:E396-402.

27. Yoganandan N, Pintar FA, Stemper BD, Wolfla CE, Shender BS, Paskoff G. Level-dependent coronal and axial moment-rotation corridors of degeneration-free cervical spines in lateral flexion. J Bone Joint Surg Am 2007;89:1066-74.

28. Yoganandan N, Stemper BD, Pintar FA, Baisden JL, Shender BS, Paskoff G. Normative segment-specific axial and coronal angulation corridors of subaxial cervical column in axial rotation. Spine (Phila Pa 1976) 2008;33:490-6.

29. Hilibrand AS, Carlson GD, Palumbo MA, Jones PK, Bohlman HH. Radiculopathy and myelopathy at segments adjacent to the site of a previous anterior cervical arthrodesis. J Bone Joint Surg Am 1999;81:519-28.

30. Rao RD, Wang M, McGrady LM, Perlewitz TJ, David KS. Does anterior plating of the cervical spine predispose to adjacent segment changes? Spine (Phila Pa 1976) 2005;30:2788-92.

31. Kolstad F, Nygaard OP, Leivseth G. Segmental motion adjacent to anterior cervical arthrodesis: A prospective study. Spine (Phila Pa 1976). 2007;32:512-7.

32. Sugawara T, Itoh Y, Hirano Y, Higashiyama N, Mizoi K. Long term outcome and adjacent disc degeneration after anterior cervical discectomy and fusion with titanium cylindrical cages. Acta Neurochir (Wien) 2009;151:303-9.

33. Anderst WJ, Donaldson WF, Lee JY, Kang JD. Subject-specific inverse dynamics of the head and cervical spine during *in vivo* dynamic flexion-extension. J Biomech Eng 2013;135:61007-8.

34. Moroney SP, Schultz AB, Miller JA. Analysis and measurement of neck loads. J Orthop Res 1988;6:713-20.

35. Pintar FA, Yoganandan N, Baisden J. Characterizing occipital condyle loads under high-speed head rotation. Stapp Car Crash J 2005;49:33-47.

36. Pintar FA, Yoganandan N, Maiman DJ. Lower cervical spine loading in frontal sled tests using inverse dynamics: Potential applications for lower neck injury criteria. Stapp Car Crash J 2010;54:133-66.

37. Seacrist T, Arbogast KB, Maltese MR, García-España JF, Lopez-Valdes FJ, Kent RW, *et al.* Kinetics of the cervical spine in pediatric and adult volunteers during low speed frontal impacts. J Biomech 2012;45:99-106.

38. Yoganandan N, Pintar FA, Maiman DJ, Philippens M, Wismans J. Neck forces and moments and head accelerations in side impact. Traffic Inj Prev 2009;10:51-7.

39. Yoganandan N, Pintar FA, Stemper BD, Schlick MB, Philippens M, Wismans J. Biomechanics of human occupants in simulated rear crashes: Documentation of neck injuries and comparison of injury criteria. Stapp Car Crash J 2000;44:189-204.

40. Wheeldon JA, Pintar FA, Knowles S, Yoganandan N. Experimental flexion/extension data corridors for validation of finite element models of the young, normal cervical spine. J Biomech 2006;39:375-80.

41. Rao RD, Currier BL, Albert TJ, Bono CM, Marawar SV, Poelstra KA, *et al.* Degenerative cervical spondylosis: Clinical syndromes, pathogenesis, and management. J Bone Joint Surg Am 2007;89:1360-78.

42. Butler JS, Oner FC, Poynton AR, O'Byrne JM. Degenerative cervical spondylosis: Natural history, pathogenesis, and current management strategies. Adv Orthop 2012;2012:916987.

43. John JD, Arun MW, Yoganandan N, Saravana Kumar G, Kurpad SN. Mapping Block-Based Morphing for Subject-Specific Spine Finite Element Models," 54th Annual Rocky Mountain Bioengineering Symposium. USA: RMBS Publishers; 2017. p. 193-9.

44. John JD, Arun MW, Saravana Kumar G, Yoganandan N. Cervical Spine Finite Element Model with Anatomically Accurate Asymmetric Intervertebral Discs. Summer Biomechanics, Bioengineering, and Biotransport Conference, ASME Tuscon, AZ; 2017. p. 153-4.